Computers and Electronics in Agriculture 151 (2018) 354–364

Contents lists available at ScienceDirect

Computers and Electronics in Agriculture

journal homepage: www.elsevier.com/locate/compag

Hydrodynamics of octagonal culture tanks with Cornell-type dual-drain system

J.M.R. Gorle[a,*], B.F. Terjesen[a], S.T. Summerfelt[b]

[a] Nofima AS, Sunndalsøra 6600, Norway
[b] The Conservation Fund Freshwater Institute, 1098 Turner Road, Shepherdstown, WV 25443, USA

ARTICLE INFO

Keywords:
Recirculating Aquaculture System (RAS)
Dual-drain
Outlet flow-split
Hydrodynamics
Computational Fluid Dynamics (CFD)
Turbulence modelling

ABSTRACT

Large culture tanks of several hundred or thousand m^3 size are generally encouraged for economic advantages in Recirculating Aquaculture Systems (RAS). Out of numerous possibilities in designing the inlet and outlet configurations in octagonal culture tanks, the inlet pipes near the corner walls and the outlets at the tank's center and/or on side wall are some of the widely-used configurations. The use of wall drain to achieve a controlled flow pattern in the tank, however, influences distinct flow features such as pressure, velocity, uniformity and turbulence in the tank, which are of theoretical interest as well as practical importance. A finite volume description of the flow in an octagonal culture tank at full-scale was therefore developed using Realizable turbulence model with second order accuracy in space and time. The tank was equipped with an inlet pipe near the corner wall and dual-drain outlet system of Cornell-type. The base case had a flow configuration of 45% of flow through central bottom drain, and the rest through the wall drain. Model verification was performed using grid convergence tests, and validation was conducted using Acoustic Doppler velocimetry (ADV) based velocity measurements. The effect of wall drain on the large-scale and small-scale turbulent structures was studied using the distribution of turbulent kinetic energy and vorticity respectively. The parametric study on the flow-split between the two outlets was analyzed using different flowfield indicators, such as flow velocity, uniformity, vorticity strength, maximum absolute vorticity and swirl number. Such an inclusive analysis not only explores the hydrodynamics in the commercial culture tanks with Cornell-type dual-drain but also recommends the farmers with the suitable flow-split between such outlet systems.

1. Introduction

In the seeking of disease prevention, increased production rates and environment preservation, Recirculating Aquaculture Systems (RAS) have been in limelight to exercise a controlled rearing system (Dalsgaard et al., 2013; Summerfelt et al., 2016). In addition to creating a healthy environment, it is possible to exert some control over the flow domain in circular-type tanks used RAS facility, which plays a critical role in fish growth and hence the production and financial benefits. Previous studies have determined that the rotational velocity about the perimeter of circular tanks is strongly dependent upon the impulse force of water flow injected tangentially into the circular-type tank (Tvinnereim and Skybakmoen, 1989; Paul et al., 1991; Davidson and Summerfelt, 2004; Oca and Masalo, 2013; Venegas et al., 2014; Plew et al., 2015; Prabhu et al., 2017; Gorle et al., 2018). Thus, rotational velocity depends upon the hydraulic exchange rate and inlet orifice velocity (dependent on orifice number, open area, and flow rate) and direction produced at the flow inlet structure(s). In contrast, rotational velocities close to the center of circular-type tanks are associated with the impulse force exiting the center of the tank, i.e., dependent upon the surface loading rate at the center drain (Davidson and Summerfelt, 2004). The inlet and outlet impulse forces are balanced by the forces created by drag on the fish and tank walls and floors (Plew et al., 2015).

The recommended hydrodynamic state of a culture tank comprises not only the sufficient rotational velocity, but also proper mixing through the occurrence of primary and secondary vortices that ensure the desired water quality. Non-uniform distribution of rotational velocity (Oca and Masalo, 2007), non-homogeneous water quality (Saba and Steinberg, 2012), and unsteady distribution of biosolids are some of the natural and undesirable phenomena occurring in culture tanks. Although there is an influence of tank geometry on the overall flow pattern (Duarte et al., 2011), the flow boundary conditions have a phenomenal impact on the hydrodynamics in the bounded space of the culture tank. Several practical methods have been tried to control the flow in the culture tank. A simple and widely adopted practice in creating a uniform inflow is to use a multiple nozzle configuration on

* Corresponding author.
E-mail address: gorle.jmr@gmail.com (J.M.R. Gorle).

https://doi.org/10.1016/j.compag.2018.06.012
Received 11 February 2018; Received in revised form 5 June 2018; Accepted 6 June 2018
Available online 20 June 2018

the inlet pipe. Oca et al. (2004) made improvements in the inlet and outlet designs to achieve the desired flow pattern in the rectangular culture tanks. The standard practice of single inlet-outlet combination, however, cannot offer a controlled flow solution that meets the flow rotationality and uniformity requirements. Instead, researchers have attempted to create adaptable boundary conditions for improved hydrodynamics (Venegas et al., 2014). Several passive flow control methods have been tested and used in the past research, which included adjustable orientation of inlet structures (Davidson and Summerfelt, 2004; and Summerfelt et al., 2004, 2006, 2009a), and baffles for better mixing of the flow (Masalo and Oca, 2014). A celebrated method is to use a multiple drain system, where more than one outlet are used at appropriate locations, to achieve desired flow conditions in the tank. In a dual-drain system with an elevated wall-drain, the solids can quickly be discharged out of the tank and improve the water quality. Also, such wall drain can reduce the flow velocity downstream and hence control the flow pattern as desired.

Although octagonal tanks are the best alternative for circular tanks with an advantage of better space management and shared sidewalls, it is important to note that there is a considerable difference between the two tank shapes as the flow velocity and water quality is concerned (Gorle et al., 2018). For instance, dead zones can be created in the near-corner wall region in the octagonal tanks, which does not happen in case of circular tanks. Circular-type culture tanks sometimes use dual-drain to create two advantages over a single drain tank, i.e., to concentrate a majority of settleable solids into a relatively small tank underflow (as in a swirl separator) and/or to shift the impulse force associated with outlet flows in a manner that can be used to help optimize water rotational velocities located in the annular region about the center of the tank (Davidson and Summerfelt, 2004; Gorle et al., 2018). Water rotational velocities, particularly within the annular region about the tank center, are critically important to create a self-cleaning tank and when trying to maintain more optimum swimming speeds for the fish. At least one drain is always located to draw flow off the bottom center of the tank. However, the second drain is typically located above the bottom-drawing drain at the tank's center (Terjesen et al., 2013) or part-way up the tank's side wall (Davidson and Summerfelt, 2004; Summerfelt et al., 2004; Despres and Couturier, 2006; Summerfelt et al., 2006; Summerfelt et al., 2009a, 2009b; Wolters et al., 2009; Pfeiffer and Riche, 2011; Carvalhoa et al., 2013; Terjesen et al., 2013; Summerfelt et al., 2016). The second drain is elevated in order to withdraw flow out of the tank in a location where it should contain minimal settleable solids, because the settleable solids tend to concentrate on the tank floor as they are moved by the tank's primary rotating and radial flows to the bottom-center drain. However, the lack of knowledge on the effect of elevated wall drain on the overall flow behavior leads to uncertain flow split ratio in the commercial as well as research facilities, which describes the paucity of research on culture tanks with dual-drain systems. Only three studies have described empirical water velocity data collected in sidewall-type dual-drain circular tanks (Davidson and Summerfelt, 2004; Summerfelt et al., 2006; Summerfelt et al., 2009a). This results in a trial-error flow-split between multiple outlets, or sometimes uncertain operating conditions in the commercial farms.

The problem of hydrodynamics in a culture tank with a single outlet at the central bottom location and tangential inflow can be viewed as the combination of rotating flow in a container that creates circular flow and vertical motion of the flow towards the outlet. Numerous theoretical and computational studies were conducted on these two cases separately in different applications, which are useful in understanding the basics of flow behavior. The case of bathtub vortex is analogous to the vertical motion of the flow in the culture tank, with throttle opened central bottom drain. The twisting air bubble swiftly penetrates into the deformed free-surface and attempts to reach the outlet at higher rotational speeds (Klimenko, 2001; Andersen et al., 2003; Mizushima et al., 2014). However, the continuous replenishment of water into the tank controls the deformation of water surface (Meshkov and Sirotkin, 2013). A relatively stable water surface can be maintained with a steady inflow rate so that the water level remains flat as well as constant. This practice simplifies the computational modelling by assuming the water surface as a stress-free boundary. Nonetheless, the additional outflow through elevated wall drain wall drain considerably influences the flowfield. Kawahara et al. (1997) observed the multiscale interactions between small-scale vortical structures that tend to wrap around the large-scale vortex column due to the local strain field. However, no research in this direction has been done on culture tank hydrodynamics.

Axisymmetric draining flow with an ideal setting of tangential inflow and central bottom outlet is apparently similar to that in a rotating tank. Flow in a stirred tank, which is predominantly tangential, was recently studied by Lane (2017) using CFD, while the particle motion in the similar systems were investigated by Bashiri et al. (2016). Particles of a wide range of size critically determine their distribution in the flowfield due to the differences in their angular velocity although the mean rotation of the flow is constant. This holds true in the case of culture tanks as well. Particles' morphology is supposed to be affected due to the shear force. When applied to fish tanks, this phenomenon is detrimental as breakup of biosolids deteriorates the water quality (Couturier et al., 2009). Improving the flow uniformity is one of the ways to reduce the extra shear on the particles in a culture tank. But, the effect of splitting flow through a center and sidewall dual-drain outlets on the flow uniformity as well as turbulence is an unexplored topic.

High-fidelity modelling, whereby the turbulent motion is resolved at high resolution using computational tools, has been a promising approach to obtain a better insight into the hydrodynamics, and thus make decisions on design improvement and optimization. Recent studies on computational modelling of hydrodynamics in a closed sea cage (Klebert et al., 2018) used unsteady Reynolds Averaged Navier-Stokes modelling to analyze the flowfield, and particle dispersion and flushing. Kim et al. (2015) performed the CFD analysis of cage systems to evaluate the flow pattern and dissolved oxygen distribution. The large eddy simulations of Salmon net cage was performed by Cornejo et al. (2014) to assess the wake dynamics and passive tracer advection in the domain. Veerapen et al. (2005) employed CFD to analyze the removal of waste solids using swirl separators.

In this study, the hydrodynamic response of a commercial culture tank as a function of flow-split between central bottom outlet and elevated wall drain was investigated using 3D CFD modelling at full-scale. Velocity measurements at discrete locations in the tank using Acoustic Doppler Velocimetry (ADV) were used to validate the computational model. Unlike the aforementioned studies, which were largely limited to the examination of global flowfield, the present study focused on the evolution of large-scale and small-scale turbulent flow structures and the effect of dual-drain system on them. Vortical field of the tank was computed using Q-criterion. Furthermore, non-dimensional flowfield indices were formulated using surface integrals to quantify the effect of dual-drain operation on the characteristics of velocity, uniformity, vortex strength, maximum circulation and swirling in the tank.

2. Recirculating Aquaculture System (RAS) tank under study

This study considered one of the nine octagonal RAS tanks at Nofima Centre for Recirculation in Aquaculture (NCRA) in Norway. The research facility was constructed to address a number of issues related to water quality, fish growth, hydrodynamics, etc., and produce an expected 480,000 smolts annually. All RAS tanks are identical in design, dimensions and equipment. To study the effect of dual-drain on the tank hydrodynamics, one of the octagonal tanks at regular operating conditions was considered in the present research. The basic dimensions of the tank are described in Fig. 1. The 100 m^3 sized tank has

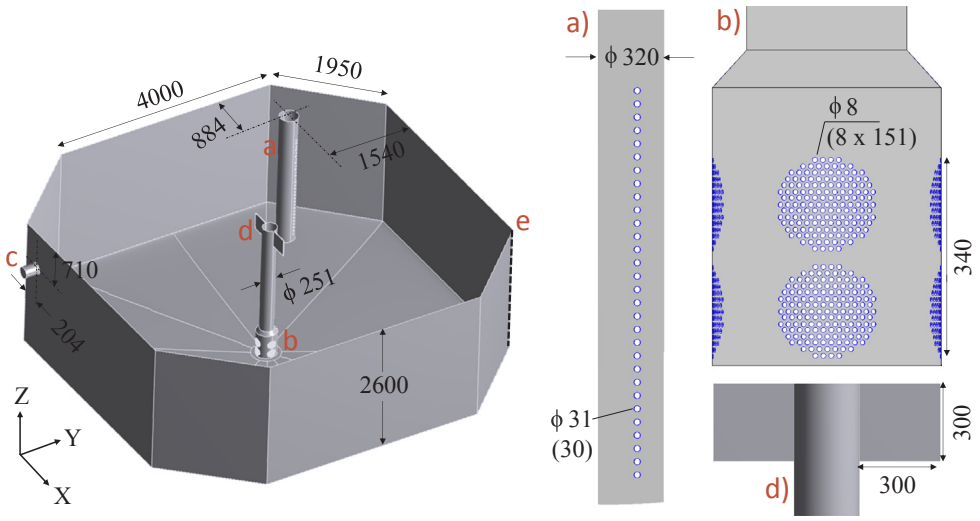

Fig. 1. Geometry definition of the culture tank. All dimensions are in mm. (a) Inlet pipe delivers the water into the tank through 30 nozzles in the direction towards the edge, *e*. The distance between the centers of successive nozzles is approximately 37 mm, and the bottom most nozzle is located at 80 mm above the floor. (b) Central outlet in the form of 8 sets of flow exit holes in 2 radial patterns. Each set has 151 holes of 8 mm each in size. (c) The wall drain of 204 mm in size is elevated to 1890 mm from the floor. (d) Two square shaped plates of 10 mm thickness are fixed on the either side of central pipe at the top to break the local vortex.

the side wall of 4 m length and corner wall of 1.95 m. Slanting floor causes the tank height increasing from 2.6 m at wall to 2.76 m at the center. The tank has an inlet pipe near the corner wall (Fig. 1a), which delivers the water into the tank through 30 nozzles, each of 31 mm in size. Flow jets, emanating from discrete inlet surfaces, quickly expand and interact with neighboring jets and thus appear to form a continuous inflow along the inlet pipe. However, the outlets are confined to specific locations, i.e. central-bottom drain (Fig. 1b), and side wall drain (Fig. 1c). The flow exiting each drain is controlled by adjusting a valve or elevation of a stand-pipe located on the piping that exited each drain. Dominant circular flow in the tank thus has to negotiate its path to exit the tank through both outlets. The rotational flow undergoes an axial motion, i.e., along the tank's height to move to the elevated outlet, which eventually creates a swirling action. Near the top of the pipe in the center of the tank, two square-shaped plates are fixed on either side of the central pipe to help reduce a local vortex (Fig. 1d). Height of the water column is 2.36 m at the wall. More details on the RAS facility design and operation can be found in Terjesen et al. (2013).

3. Methodology

3.1. Experimental measurements

One of the challenges in developing the computational models of a full-scale industrial flow system is concerned about the model accuracy due to a number of simplifications made in the definition of geometry and boundary conditions. Experimental validation is therefore pivotal to obtain a reliable CFD solution, which was done in the present study using Acoustic Doppler Velocimetry (ADV). The test rig contained a Nortek three-dimensional ADV vector, which works on the principle of Doppler shift. The acoustic transmitter at the center of probe's head sends a pulse, which gets reflected by air bubbles and suspended solid particles in the water. The three receivers around the transmitter, placed at an azimuthal distance of 120° from each other, receive the reflect the acoustic signals from the sample volume, 10 cm below the transmitter. The reflections experience a Doppler shift due to the velocity difference between the scattered particles and the probe. The radial velocities are monitored by the processing module of the instrument, which are then converted into Cartesian coordinates. An analogue electronic system on a portable computer performs signal processing computations to deliver the 3D velocity components and the signal properties at a maximum frequency of 64 Hz. The ADV instrument was mounted vertically downwards into the tank at each of predefined locations, which are shown in Fig. 2. A total of 36 measurements was performed at three depths i.e., 15%, 36% and 58% of water

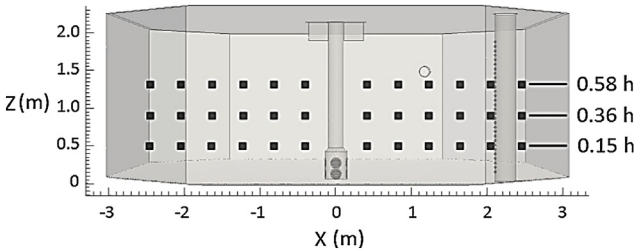

Fig. 2. Discrete locations in the tank for velocity measurements. 12 points at each of 3 depths were selected on the measurement plane y = −0.1 m. Water column height, h, is 2.36 m.

column height. Each pair of points was half a meter apart horizontally. The walkway at the top of the tank along the center enabled to measure the velocity across the plane, y = −0.1 m. The data quality was assessed using the correlation between the radial velocity components, which was above 80% in all measurements. The data was collected at base case operating conditions, which corresponded to the inlet flow rate of 2500 L/min, and mean hydraulic retention time of 40 min. The objective of this study was to develop the computational model to anchor the experimental data of this operating point with specific boundary conditions, and continue the predictions of flowfield with other boundary conditions.

3.2. Computational framework

The computational modelling of culture tank hydrodynamics requires the extraction of a fluid body from the tank's geometry, finite volume discretization, solution process for turbulence modelling and visualization and analysis of numerical results. A consistent and cost-effective computational framework was used in the present study.

3.2.1. Pre-processing

The CAD software, CATIA V5 (Dassault Systems, France), which was used to generate the assembly model of the tank, is capable of creating an efficient and error-free formats of a solid model, compatible for different computational platforms. In addition to the basic CAD features such as solid-based, surface-based, boolean and assembly operations, CATIA enables to merge and smoothen the surfaces as required so that a reliable cohesive input CAD data can be exported to a simulation platform. One of the limitations of CATIA V5 is that its export options doesn't include the Parasolid, which was required for the simulations in the present study. An external CAD translator, 3D-tool was therefore employed for CAD format conversion.

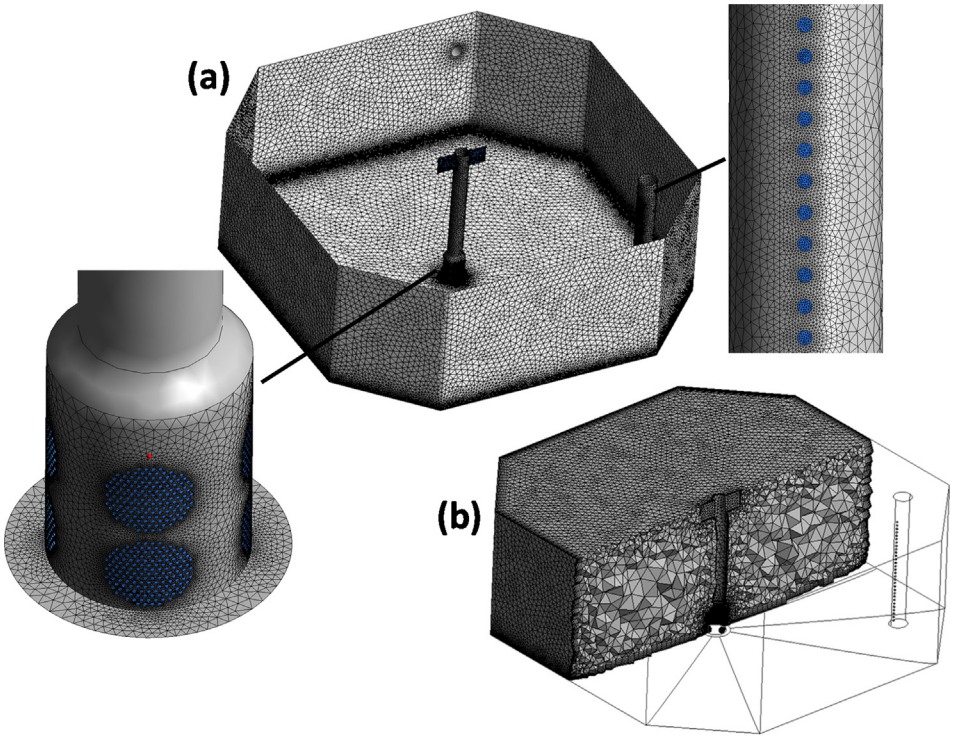

Fig. 3. Visualization of unstructured mesh. (a) Triangular surface mesh, with enlarged views of inlets and outlet surfaces, and (b) tetrahedral volume mesh slice.

Considering the geometrical complexity, an unstructured mesh was generated using the automatic mesh generator, Castnet (DHCAE Tools GmbH, Germany). The combined hexa-prism grid topology was maintained to negotiate the structural continuity for high quality distribution of cells. Fig. 3 shows the surface and semi-volume mesh visuals. The in-built utilities to identify and treat the undesired geometrical entities, such as slivers, open edges and small features, enabled smoother meshing process and better distribution of cells. The quality of the mesh was thoroughly checked for element aspect ratio, orthogonality and dihedral angle of the cells. The maximum aspect ratio was 68 with over 95% of cells having less than 30. 93% of the cells have the dihedral angle between 70° and 120°. 9% of the domain has cells with the skewness greater than 0.85. Although the meshing of larger volumes with a wide range of geometrical scales as in the present case cannot generate a perfectly discretized flow domain, persistent testing against mesh resolution and quality metrics should produce identical results. A number of grids were tested to ensure the mesh independency, and the validated results are presented in Section 4.1.

3.2.2. Turbulence modelling

The instantaneous flow variables in a turbulent flow are decomposed using the Reynolds averaging $\Phi_i = \overline{\Phi_i} + \Phi_i'$, where $\overline{\Phi_i}$ and Φ_i' are the mean and fluctuating components of i^{th} flow variable. The governing equations to solve the time-averaged incompressible flowfield are

$$div\,\Phi = 0$$

$$\dot{\bar{\Phi}} = -\frac{1}{\rho} grad\,\bar{p} + \nu\Delta\bar{\Phi} - div\,\tau$$

Here, the Reynolds stress tensor $\tau = \overline{\Phi' \otimes \Phi'}$ appears due to the averaging of non-linear convective fields. The solution for this closure problem is to eliminate the fluctuating component Φ' in the expression for Reynolds stress tensor. The closure approximation according to Boussinesq and gradient-diffusion hypotheses (Boussinesq, 1897; Schmitt, 2007) can be written as

$$\tau = \frac{2}{3}kI - \nu_t \mathscr{S}$$

where $k = \frac{1}{2}\overline{|\Phi'|^2}$ is the turbulent kinetic energy, I is the identity tensor, ν_t is the turbulent viscosity and $\mathscr{S} = \frac{1}{2}[grad\,\bar{\Phi} + (grad\,\bar{\Phi})^T]$ is the mean stretching tensor. Thus, the flow conservation equations read

$$div\,\Phi = 0$$

$$\dot{\bar{\Phi}} = -\frac{1}{\rho} grad\left(\bar{p} + \frac{2}{3}\rho k\right) + (\nu + \nu_t)\Delta\bar{\Phi}$$

A wide range of solutions methods, from very simple to highly exotic, are available to model the turbulent viscosity. Although Large Eddy and Direct Numerical Simulations are known for their better performance (Baerenzung et al., 2010, Dai et al., 2015) than universal two-equation turbulence models, the industrial applications cannot afford the CPU effort involved in such computations. In this study, Realizable k–ε turbulence model (Shih et al., 1995) was used to solve the following transport equations for turbulent kinetic energy k and its dissipation rate $\varepsilon (=2\nu\,\overline{\mathscr{S}'}:\overline{\mathscr{S}'})$.

$$\frac{\partial}{\partial t}\rho k + \frac{\partial}{\partial x_j}(\rho k u_j) = \frac{\partial}{\partial x_j}\left[\left(\mu + \frac{\mu_t}{\sigma_k}\right)\frac{\partial k}{\partial x_j}\right] + P_k - \rho\varepsilon - Y_m + S_k$$

$$\frac{\partial}{\partial t}\rho\varepsilon + \frac{\partial}{\partial x_j}(\rho\varepsilon u_j) = \frac{\partial}{\partial x_j}\left[\left(\mu + \frac{\mu_t}{\sigma_\varepsilon}\right)\frac{\partial \varepsilon}{\partial x_j}\right] + \rho C_1 S_\varepsilon - \rho C_2 \frac{\varepsilon^2}{k + \sqrt{\nu\varepsilon}} + C_{1\varepsilon} C_{3\varepsilon} P_k \frac{\varepsilon}{k} + S_\varepsilon$$

Here, $C_1 = \max\left[0.43, \frac{\eta}{\eta+5}\right]$, $\eta = \sqrt{2S_{ij}S_{ij}}\frac{k}{\varepsilon}$.

Thus, the realizability in this two-equation model is enforced by the formulation of μ_t, which confers that C_μ is not a constant but related to the strain tensor. Realizable k-ε model is also considered superior to the standard k-ε model, developed by Jones and Launder (1972) Launder and Spalding (1974), as the former accounts for strong streamline characteristics associated with the flow rotations and vortices, which are natural phenomena in the large flow domains like culture tanks.

3.2.3. Numerical approach

Water was the working fluid. The nozzle surfaces on the inlet pipe were assigned with mass flow inlet condition. In the base case, the mean hydraulic time (HRT) of the tank was 40 min, which corresponded to the inlet mass flow rate of 42 kg/s. Wall drain was applied the mass flow outlet with 55% of the total flow through it, while the holes on the bottom of central pipe were applied pressure outlet. Water surface was treated as a flat stress-free wall. The solid boundaries of the tank were given no-slip wall condition.

The unsteady incompressible 3D solver was used in the computations. Gaussian linear scheme was used to discretize the convective and diffusive terms to second order accuracy in space and time. Enhanced wall treatment was applied to model the viscous layers in the near wall region. Therefore, the non-dimensional wall distance y+ was maintained in the range of 0.8–1.7. Geometric Agglomerated Algebraic Multigrid (GAMG) method was defined to solve the pressure equation, and Semi-Implicit Method for Pressure Linked Equations (SIMPLE) algorithm was used to couple the pressure and velocity equations. Gauss-Seidel smoother with *smoothSolver* scheme was used to solve the other flow equations. The convergence criteria were defined to have 1E-5 as minimum per iteration, while 1E-3 was the maximum observed residual value. As noted by Aubin et al. (2004), anisotropic turbulence definition for high Reynolds number flows with higher order discretization is likely to diverge the solution. The under-relaxation factors were lowered during initial time steps, which were subsequently raised after a stable solution was achieved. A fixed time step of 0.01 s was used with 25 inner iterations. Intel Xeon E5-2683 v3 2.00 GHz workstation with 28 cores was used to run the simulations in parallel mode.

4. Results

4.1. Verification and validation

Although the ADV based velocity measurements could offer an empirical base to validate the computational findings, the experimental setup itself contributes to measurement errors and uncertainties, which is usual in most industrial systems with complex flow patterns. The uncertainty in the velocity measurements was therefore analyzed by taking the standard deviation, σ, of output signal. Higher uncertainty was found in the measurements near the walls, where the flow had relatively higher velocity. The highest deviation in the measurements was 4.8 for the mean velocity of 39 cm/s and the lowest deviation was 1.9 where the mean was 34.5 cm/s magnitude. This admits a sufficient accuracy of the ADV measurements in culture tank experiments (Masalo et al., 2008; Gorle et al., 2018). The major non-linearity in the flow domain in the form of vortex column was not only reported in the measurement deviation within half of the tank's radial distance, but also reflected in the discrepancy between the experimental and corresponding computational results. More information on vorticity field in the tank is presented in Section 4.3.

The resolution of the computational grid should be sufficiently fine to ensure the solution accuracy. However, large 3D meshes require more CPU time for the solution to converge. A trade-off between the computational effort and result accuracy is therefore necessary. Since the main focus of the study was on the hydrodynamic analysis at full-scale of a large water body, the impact of mesh size on velocity magnitude was assessed to investigate the mesh independency. A number of grids with same topology and near-wall treatment, but with successive refinement using base cell size, were tested by comparing the normalized velocity (V/V_0) along the each of the measurement depths across $y = -0.1$ m. Here, V_0 is the inlet nozzle flow velocity. This was calculated from the volume flow rate through the inlet pipe, which was measured by means Portaflow 300 Ultrasonic Flowmeter. Fig. 4 compares the performance of three selected meshes - 1, 2 and 3, which produced less than 1% variation in the normalized velocity profile. The mesh with at least 752,848 cells was able to produce reliable flow predictions, and further increase in the mesh size was no longer considerably altering the field variables. The flow from inlet reaches the negative-X side and undergoes a gradual momentum diffusion before reaching the positive-X side. The resulting velocity difference between $x/X = -0.8$ and $+0.8$ of approximately 11% indicates an asymmetry in the flow pattern. Although the CFD findings were nearest to the experimental measurements, and both approaches produced identical velocity trends across the tank, the maximum discrepancy was still approximately 12% near the walls and mid-radius location at $z = 0.58$ h, and the computational predictions did not lie within measurement deviations. Near the periphery i.e. $0.6 < |x/X| < 1$, the difference between ADV and CFD was fairly constant at the selected heights of water column, this discrepancy near the tank's center likely increased with the height. Within the half-radius reach from the center, the deviations of computational predictions from experimental results were approximately 35% and 65% more at $z = 0.36$ h and 0.58 h compared to that at $z = 0.15$ h. Otherwise, the computational predictions either fell within the error bars or deviated by less than 10% from the mean values of the measurements.

4.2. Effect of wall-drain

In addition to the inlet near the corner wall that discharges the flow in a diagonal direction, the elevated wall drain also creates nonlinear flow conditions in the tank. This concern is more crucial when the flow split between the central outlet and wall drain is uncertain, and the flow pattern is not completely predictable. Therefore, a comparison was made between the extreme tank-draining cases i.e. 100% flow exiting through bottom-central drain, and 100% flow exiting through wall drain. The flow-split ratio, *s*, is defined as the ratio of the flow rate of central drain to that of wall drain. Therefore, the cases of pure central drain and pure wall drain correspond to *s* equal to 1 and 0, respectively. In addition, an intermediate draining case for $s = 0.45$ was considered, which constituted the base case. The distribution of large-scale turbulent structures in a fully-developed turbulent state of the three cases is presented in Fig. 5. The visualization of turbulence clutter was minimized to turbulent kinetic energy, $k \in [0.003, 0.3]$, which enabled the analysis of a continuous structure of turbulence happening in the flow domain. Higher intensity of Reynolds shear stresses creates larger turbulent structures, which contributes to increased production of turbulent kinetic energy. The iso-surfaces represent significant portion occupied by *k* in the total kinetic energy. The non-uniform distribution of *k* indicates an intensive flow mixing near the inlet nozzles and near-downstream, and a lesser mixing action in the core of the tank. However, the accelerated flow near the central drain in operation produced *k* around the outlet (Fig. 5b), which steadily reduced with the outflow through wall drain (Fig. 5a), and became negligible with pure wall drain configuration (Fig. 5c). In addition, the wall drain flow impedes the convective transport mechanism of strain energy in the rotational flow of the tank, which results in a locally reduced *k* (Fig. 5a and c). Looking at the streamline pattern on the central vertical plane, the pure central drain case has the vortices attached to the central pipe, which explains the existence of vortex column in this location. In case of wall drain, particularly pure wall drain, these central vortices appear to get detached from the central pipe, which means that the characteristics of vortex column change. More details on this are available in Section 4.3.

For further evaluation of flowfield along the tank's height, three horizontal planes are considered; one is close to the tank's floor ($z = 0$) that covers the flow through the central outlet, second is at $z = 0.5$ h, which is at mid-height of the tank, and the third is at $z = 0.7$ h, which passes through the wall drain of the tank. Fig. 6 compares the three draining configurations for the distribution of tangential and radial velocity components, V_θ and V_r respectively, plotted along three radial lines L_1, L_2 and L_3 on the selected planes. The velocity components are normalized by the nozzle inlet velocity V_0. The negative portion of horizontal axes represents half of respective line where the line

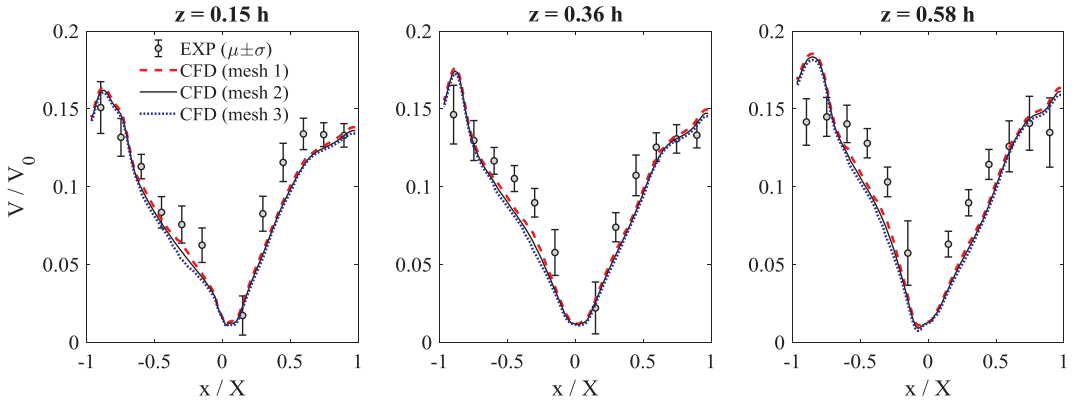

Fig. 4. Comparison between the experimental and computational results of normalized velocity at three depths of the tank along y = −0.1 m. Meshes 1, 2 and 3 had 752,848, 891,346 and 1,016,792 cells, respectively.

numbers are mentioned in the reference plan view. It is noticed that, irrespective of the outflow design, the average distribution of V_θ is approximately ten times higher than that of V_r. The variation in the distribution of V_r along the height of water column is more significant than that of V_θ. Fig. 6 highlights how the strong primary rotating flow, V_θ, creates more substantial radial flows, V_r, on the planes closer to the top elevation and bottom elevation, while the plane at mid-tank elevation had somewhat weaker V_r. In addition, the pure wall drain configuration produces generally stronger V_r than in the pure center drain configuration. The immediate downstream location of L_1 from the inlet apparently makes it to have higher V_θ than the lines L_2 and L_3, which are located further downstream. The shortest line L_3 appears to have a relatively more uniform distribution of V_θ near the walls, which is due to the momentum conservation. The profiles of V_θ along the positive portions of L_2 and L_3 is likely identical in all cases, with a little difference between them on Plane 3, where there is a flow through wall drain.

4.3. Parametric study on outlet flow split

The rotational motion of the fluid at high Reynolds number in a circular or octagonal culture tank is dominated by axisymmetrical vortices of different structures and length scales, which can influence the mean flow. Fig. 7(a–k) describes the effect of flow-split ratio, *s*, on the vorticity distribution across the tank through a parametric study on the central drain flow ranging from 100% to 0 with 10% decrement. Coherent vortices were identified using Q-criterion, which is defined by the positive second invariant of velocity curl (Gorle et al., 2016). Before exploring the effect of wall drain on the vortex dynamics, it is important to understand the two modes of interaction between the prevailing vortical structures; stretching and stripping (Marshall and Beninati, 2005; Candon and Marshall, 2012). In the vortex-dominating base case, as depicted in Fig. 7(a), the major vortical features are broadly classified as vortex column (C), vortex ring (R) and vortex filament (F). Vortex filaments shedding from the tank walls due to vortex-solid interaction convect in the direction of the flow and wrap around the vortex column and ring. The immobility of the vortex column is reasonably explained by the steady boundary conditions in a confined domain. The vortex column could however not be recognized as a perfect axisymmetric cylinder but a semi-closed and skewed contour, which is due to the eccentric placement of inlet pipe, the discharge of inflow in diagonal direction and non-uniform evolution of secondary flows around the vortex core. Although the filaments seem to align in the direction of tangential velocity, their self-induced velocity attempts to sweep themselves towards the vortex column. In addition to self-induced velocity, the local turbulence intensity plays a vital role in stretching the filaments and entrain them into the vortex column. The vortex ring, R, is another critical structure that plays an important role in stripping or slicing off the central vortex column. In the present case, it is evident that the vortex ring has sufficient strength to result in an exchange of fluid between the vortex column and its surroundings. It is therefore necessary to underline that there is an appreciable influence of turbulence field on the enstrophy structures in the tank and any change in the boundary conditions can directly affect the flow physics. Enstrophy is the integral of the vorticity and it is proportional to the rate of decrease of the energy of a fluid flow. Evolution and dynamics of coherent structures were found to be changing gradually from pure central drain case to pure wall drain case. Referring to pure central drain as depicted in Fig. 7(a), the rotating flow exiting through the bottom outlet plays a dominant role in preserving the geometry of the vortex column. For the flow split ratio, *s*, from 1 to 0.7 i.e. Fig. 7(a–d), the major observation was the gradual destruction of vortex column.

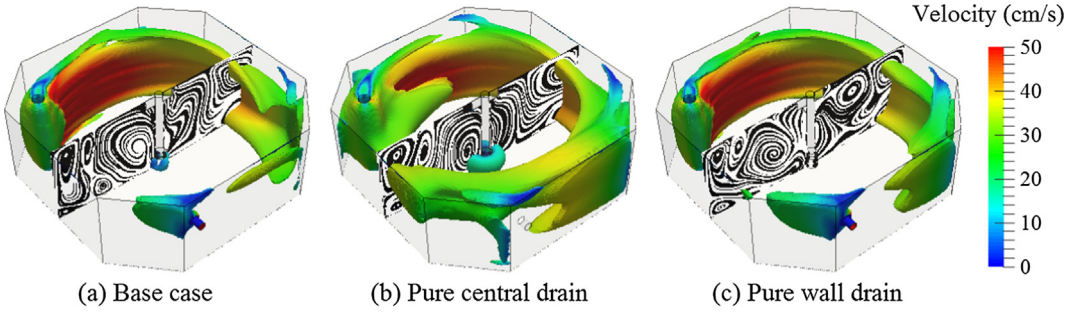

Fig. 5. Comparison between different outflow options using integrated flowfield representation of intensified 3D turbulent kinetic energy, *k*, and streamline distribution on central vertical plane. Iso-surface of *k* is colored on the scale of velocity magnitude. Planar streamlines highlight the prevalence of secondary vortices that promote mixing action in the tank through tea-cup hydrodynamic effect. (For interpretation of the references to colour in this figure legend, the reader is referred to the web version of this article.)

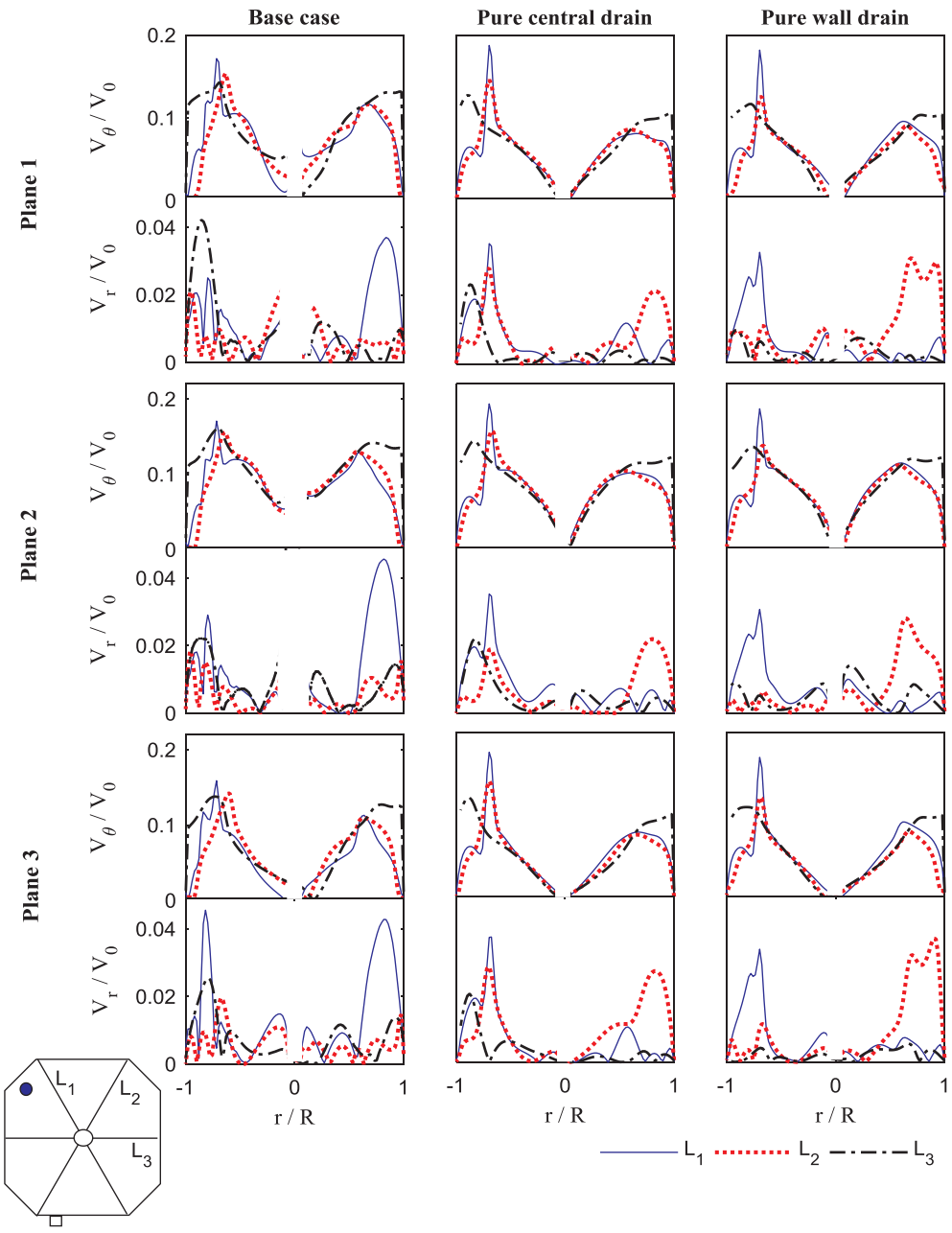

Fig. 6. Comparison between the base case (s = 0.45), pure central drain (s = 1) and pure wall drain (s = 0) configurations for the distributions of velocity components across the Plane 1 (z = 0), Plane 2 (z = 0.5 h) and Plane 3 (z = 0.7 h). Magnitudes of tangential and radial velocities are plotted along three radial lines, L_1-L_3, which are at every 60° angular distance on each plane. Inlet pipe is highlighted in blue, which creates a clockwise flow pattern when viewed from top. Negative portion of X-axis in each plot represents the side where the line numbers are mentioned (left bottom corner). (For interpretation of the references to colour in this figure legend, the reader is referred to the web version of this article.)

With these dynamics continued, the vortex regime state underwent a sudden stretching mechanism for s = 0.6. With 60% flow through the central drain and the rest through the wall drain, approximately 10% increase in the size of the vortex ring, R, was observed (Fig. 7e), and then remained fairly unchanged with further lower s values (Fig. 7f–k). Interaction between the vortex ring and intense turbulence structures due to the inlet flow is responsible for the cascade process, whereby the large-scale features breakdown to smaller, and the small-scale structures become smaller with stronger enstrophy. On the other hand, the kinematic mechanism of vortex stretching was equally observed at the bottom of the vortex column, C, which increased by 9% in size, when s was reduced from 0.7 to 0.6 (Fig. 7e). However, the imposed strain due to the wall drain flow on the vortex column caused it to collapse with s lower than 0.5 (Fig. 7g–k), and continued until a vortex streak was left at s = 0 (Fig. 7 k). Another major observation is about the strength of vorticity; more flow through wall drain, lesser intensified the vortex ring is. However, the concave shape of the ring around the column when viewed from the outside was undisturbed.

The design of rearing tanks usually focuses on creating a desirable flow pattern with sufficient water velocity to provide optimal swimming speeds for the fish, to rapidly flush settleable solids through the tank's bottom central drain, and to avoid the sedimentation of biosolids. In addition to the flow momentum, the gravitational force is a major contributor to the motion of the solids in the culture tanks. Settleable solids are kept moving above the floor of the tank by the strong primary rotating flow, V_θ, while the much weaker radial flows, V_r, keep the settleable solids moving towards the drain located at the bottom-center of the tank. Quiescent zones near the tank's floor are detrimental because the particles tend to settle faster as they descend from upper region. These settleable solids can collect on the tank floor if velocity is insufficient. Fig. 8(a) shows the normalized velocity magnitude along the tank's height for full range of wall-drain flows. Pure wall drain design displays the lowest velocity, particularly near the bottom-center of the tank, which gradually increases with the increase in the flow through central drain. This suggests that a quiescent zone that collects settleable solids could form about the bottom-center of the tank as the

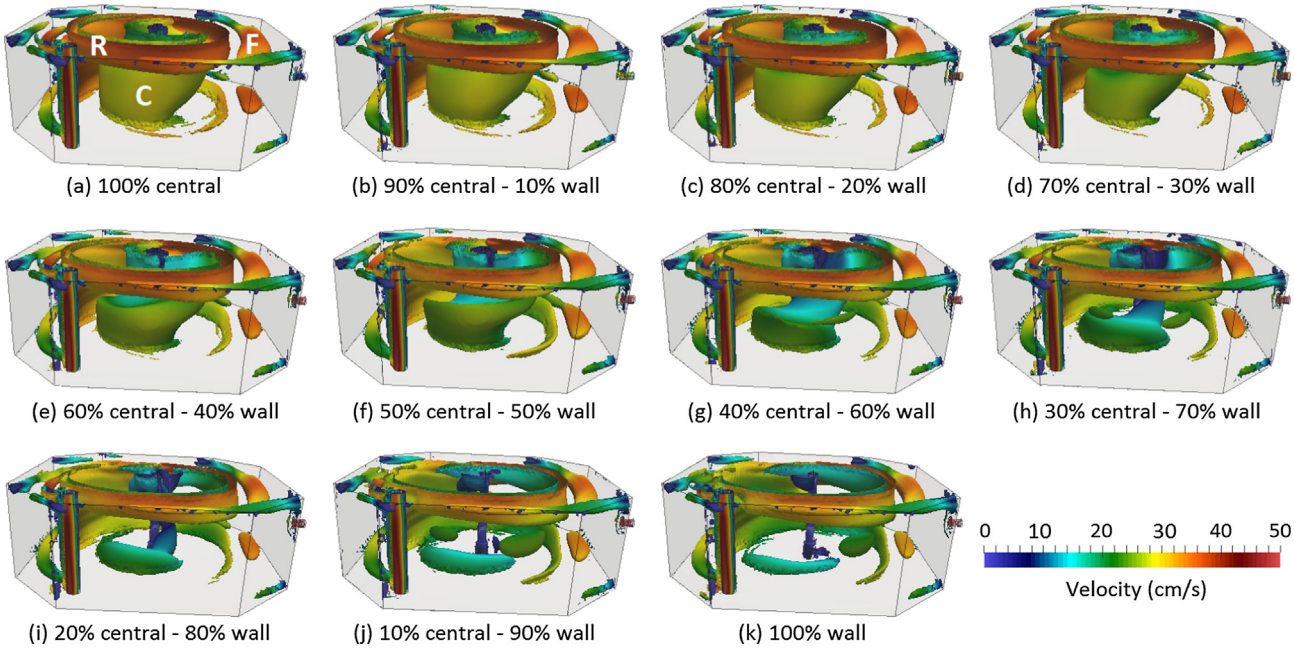

Fig. 7. Effect of flow-split ratio, *s*, on the vorticity field in the tank. Figures (a)–(k) correspond to *s* from 1 (pure central drain) to 0 (pure wall drain) with 0.1 common difference. Coherent vertical structures are visualized using iso-surfaces with Q = 0.02, colored on the scale of velocity magnitude. A steady decrease in the height of vortex column C, increase in the number of vortex filaments F and decrease in the intensity of vortex ring R are evident with the decreasing *s*. (For interpretation of the references to colour in this figure legend, the reader is referred to the web version of this article.)

flow split to the tank wall drain approaches 100%. Pure central drain, which does not obstruct the rotation as the wall drain does, provides approximately 25% of higher velocity in the tank. Also, the velocity-drop near the floor is decreased by approximately 2% in case of pure central drain case, compared to the pure wall drain case. When looking at the effect of wall drain in controlling the flow velocity in the tank, 10% decrease in the average velocity across the Plane 3 for the base case (55% flow through wall drain) and 19% decrease for pure wall drain case is observed. However, the advantage of flow control using the wall drain penalizes the flow uniformity, which is one of the judging factors in the designing process of a culture tank. The quantification of flow uniformity was made using the index γ (Gopaliya et al., 2011; Nordin et al., 2017), which is defined as

$$\gamma = 1 - \frac{1}{2nA}\sum_{i=1}^{n}\frac{\sqrt{(V_i - \bar{V})^2}}{\bar{V}}A_i$$

where n is the number of cells in the section of area A, V_i is the velocity in the cell, whose area is A_i and $\bar{V}$ is the area-weighted mean velocity across the surface. Fig. 8(b)shows the variation in flow uniformity across the water column height for different *s* values. The operation of wall drain deteriorates the flow uniformity by 5.5% on average, with a steeper decrease in γ for *s* beyond 0.3. This is possibly due to the fact that the operation wall drain creates a vertical flow motion in a dominantly rotating flow, which increases the non-uniform flow features. However, the flow is locally more uniform near the wall drain, which is evident from the peak of γ-surface at 0.7 h for pure wall drain configuration. The flow structure is relatively less uniform near the floor and water surface.

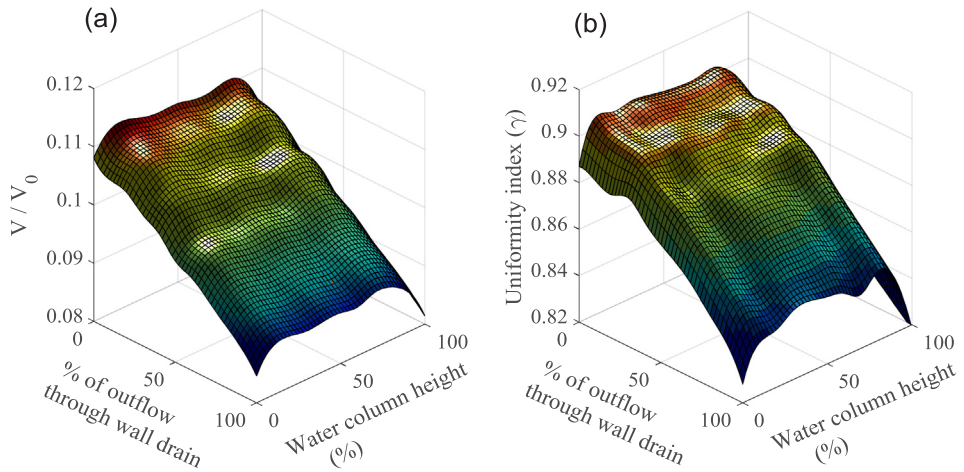

Fig. 8. Effect of wall drain on the normalized flow velocity (left) and uniformity index γ (right) along the height of water column.

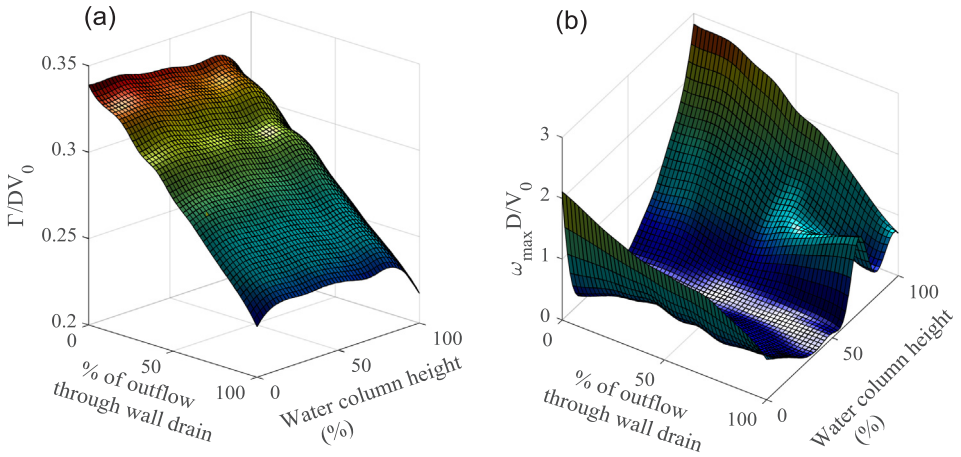

Fig. 9. Effect of wall drain flow on the vorticity strength (left) and maximum absolute vorticity (right) across the height of water column. Split-ratio, *s*, has a fairly linear relationship with vorticity strength, and a non-linear relationship with maximum vorticity.

To quantify the effect of flow-split ratio, *s*, on the dynamics of vortex house - an influencing phenomenon of the global flowfield, the variation of circulation Γ ($= \int_A \omega dA$) was computed, where ω is the angular velocity. The circulation, normalized by DV_0, for different values of *s* is plotted in Fig. 9a. Here, D is the characteristic length, which is the tank's equivalent diameter, and V_0 is the nozzle flow velocity. The numerical dissipation was not assessed in this regard, assuming that the vortex dissipation was purely due to the viscous effects during transportation mechanism. The decreasing trend of vortex strength with the amount of outflow through wall drain indicates a possible increase in the characteristic length of effective planar vortex at a given water column height. In case of pure wall drain, the lowest ω near the tank's floor causes a lower circulation locally. Apart from a little increase near the tank's floor and a damp near the water surface, the vortex strength doesn't vary considerably along the height of water column. While the planar vorticity strength, being an integral value, appears to be changing linearly with *s*, the maximum value of absolute vorticity, ω_{max} is purely dependent on the local vortex strength, which explicitly reveals the effect of flow through wall drain on the flowfield. Referring to Fig. 9(b), the peak values of maximum vorticity were observed near the water surface, followed by those near the tank's floor. The lowest values were approximately at mid-height of the tank. With 50% or more flow through the wall drain, ω_{max} at 0.7 h sharply increases and reaches the highest in the case of pure wall drain, which represents an additional production of vorticity due to the flow turning into the wall drain. This nonlinearity in the normalized ω_{max} near the wall drain would result in the vortices of different sizes. Furthermore, a gradual decrease in ω_{max} was noticed from the case of pure central drain to that of pure wall drain by 68% and 75% near the floor and water surface, respectively.

The combined tangential and axial motion of the fluid in the tank generates a swirling action. Although the tangential component is much larger than the axial and radial components, the spatial gradients of latter are greater than that of the circumferential velocity. An appropriate measure for the degree of swirling motion is the swirl number (S_n), which is defined as

$$S_n = \frac{\int_0^R r^2 V_\theta V_z dr}{R \int_0^R r V_z^2 dr}$$

where *R* is the radial distance from the tank's center (Al-Zurfi and Turan, 2015). The above definition shows that the swirl number is an integral quantity of the flowfield and it is important to note that different velocity distributions can have the same swirl number. Thus, the swirl number cannot provide the full characteristics of the swirling flow, but gives a global indication of swirl intensity in the tank. As shown in Fig. 10, the swirl level is higher close to the tank's floor than

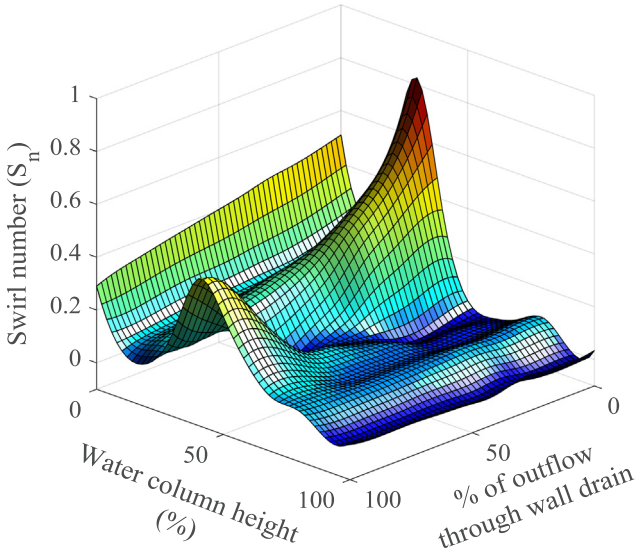

Fig. 10. Variation of swirl number along the height of the water column with the amount of outflow through wall drain.

at the water surface. This 3D surface shows the highest S_n at approximately between 70 and 80% of the tank's height with pure central drain, which is possibly due to the maximum axial flux of angular momentum. The lower axial flux of axial momentum at approximately 60% of tank's height with pure wall drain due to the tendency of the flow to exit from here caused the second peak of S_n at this location. Another observation is that the bottom half of the tank comprises more dynamic swirling motion than the upper half.

5. Conclusions

To the authors' knowledge, the ever first high-fidelity study on the effect of dual-drain on the culture tank hydrodynamics was conducted in this research. The Cornell-type dual-drain system in an octagonal culture tank of 100 m^3 at Nofima Centre for Recirculation in Aquaculture (NCRA) was investigated using the turbulence modelling technique. A good match between the computational and experimental results was achieved, which confirmed the validity of the CFD model. The effect of flow split between multiple outlets on the overall hydrodynamics is obvious. Tank with conventional central outlet on the floor essentially creates the vortex column, which is likely destructed by the operation of wall drain. In the limiting case of pure wall drain, the vortex column disappeared with a 25% reduction in the rotational flow

velocity. This resulted in a skewed flow patter in the tank, which has 5.5% lesser average uniformity. While the operation of wall drain has a fairly linear effect on the flow velocity, uniformity and vortex strength, it shows a non-linear influence on the maximum absolute vorticity and swirl number across the tank height.

This study, to some extent, explored the *modus operandi* of elevated wall-drain in terms of the evolution of vortical structures and swirl flow parameters, but proximate causes of variations in the flow physics deserve a further qualitative research. Although commercial culture tanks are preferred to operate at a mean hydraulic retention time of 45–50 min, the possible HRT varies between 35 and 170 min (Summerfelt et al., 2016). The Reynolds effect on the vorticity distribution, flow uniformity, the evolution of turbulence parameters and particle distribution are yet unknown, and need to be investigated. The purpose of vortex breaker on the central pipe is to control the local flow *passively*. This device was, however, ineffective in controlling the vortex column because the size of the vortex column exceeded the dimensions of vortex breaker. Consideration of Reynolds number, Weber number and Froude number in designing an appropriate vortex breaker will possibly change the effectiveness of wall drain in controlling the overall flow pattern in the tank.

Acknowledgements

This research was part of the CtrlAQUA SFI, Centre for Closed-Containment Aquaculture, and funded by the Research Council of Norway (project #237856/O30) and the CtrlAQUA partners. The authors thank Britt Kristin Megard Reiten of Nofima AS for assistance with the velocity measurements.

References

Andersen, A., Bohr, T., Stenum, B., Rasmussen, J.J., Lautrup, B., 2003. Anatomy of a bathtub vortex. Phys. Rev. Lett. 91 (10), 104502. http://dx.doi.org/10.1103/PhysRevLett.91.104502.

Al-Zurfi, N., Turan, A., 2015. A numerical simulation of the effects of swirling flow on jet penetration in a rotating channel. Flow Turbulence Combust. 94 (2), 415–438. http://dx.doi.org/10.1007/s10494-014-9586-9.

Aubin, J., Fletcher, D.F., Xuereb, C., 2004. Modeling turbulent flow in stirred tanks with CFD: the influence of the modeling approach, turbulence model and numerical scheme. Exp. Therm. Fluid Sci. 28 (5), 431–445. http://dx.doi.org/10.1016/j.expthermflusci.2003.04.001.

Baerenzung, J., Mininni, P.D., Pouquet, A., Politano, H., Ponty, Y., 2010. Spectral modeling of rotating turbulent flows. Phys. Fluids 22, 025104. http://dx.doi.org/10.1063/1.3292008.

Bashiri, H., Alizadeh, E., Bertrand, F., Chaouki, J., 2016. Investigation of turbulent fluid flows in stirred tanks using a non-intrusive particle tracking technique. Chem. Eng. Sci. 140, 233–251. http://dx.doi.org/10.1016/j.ces.2015.10.005.

Boussinesq, J., 1897. Theorie de l'ecoulement tourbillonnant et tumultueux des liquides. Gauthier-Villars et fils, Paris.

Candon, S., Marshall, J.S., 2012. Vortex ring deformation, capture, and entrainment by a columnar vortex. Phys. Fluids 24 (9), 093604. http://dx.doi.org/10.1063/1.4753946.

Carvalho, R.A.P.L.F., Lemos, D.E.L., Taconb, A.G.J., 2013. Performance of single-drain and dual-drain tanks in terms of water velocity profile and solids flushing for in vivo digestibility studies in juvenile shrimp. Aquacult. Eng. 57, 9–17. http://dx.doi.org/10.1016/j.aquaeng.2013.05.004.

Cornejo, P., Sepulveda, H.H., Gutierrez, M.H., Olivares, G., 2014. Numerical studies on the hydrodynamic effects of a salmon farm in an idealized environment. Aquaculture 430, 195–206. http://dx.doi.org/10.1016/j.aquaculture.2014.04.015.

Couturier, M., Trofimencoff, T., Buil, J.U., Conroy, J., 2009. Solids removal at a re-circulating salmon-smolt farm. Aquacult. Eng. 41 (2), 71–77. http://dx.doi.org/10.1016/j.aquaeng.2009.05.001.

Dai, Y.-J., Huang, W.-X., Xu, C.-X., Cui, G.-X., 2015. Direct numerical simulation of turbulent flow in a rotating square duct. Phys. Fluids 27, 065104. http://dx.doi.org/10.1063/1.4922087.

Dalsgaard, J., Lund, I., Thorarinsdottir, R., Drengstig, A., Arvonen, K., Pedersen, P.B., 2013. Farming different species in RAS in Nordic countries: current status and future perspectives. Aquacult. Eng. 53, 2–13. http://dx.doi.org/10.1016/j.aquaeng.2012.11.008.

Davidson, J., Summerfelt, S.T., 2004. Solids flushing, mixing, and water velocity profiles within large (10 and 150 m3) circular 'Cornell-type' dual-drain tanks. Aquacult. Eng. 32 (1), 245–271. http://dx.doi.org/10.1016/j.aquaeng.2004.03.009.

Despres, B., Couturier, M., 2006. Hydrodynamic characteristics of multi-drain circular tanks. In: 6th International Recirculating Aquaculture Conference, July 20–23, Roanoke, Virginia, pp. 394–404.

Duarte, S., Reig, L., Masalo, I., Blanco, M., Oca, J., 2011. Influence of tank geometry and flow pattern in fish distribution. Aquacult. Eng. 44 (2), 48–54. http://dx.doi.org/10.1016/j.aquaeng.2010.12.002.

Gopaliya, M.K., Goel, P., Prashar, S., Dutt, A., 2011. CFD Analysis of performance characteristics of S-shaped diffusers with combined horizontal and vertical offsets. Comput. Fluids 40, 280–290. http://dx.doi.org/10.1016/j.compfluid.2010.09.027.

Gorle, J.M.R., Chatellier, L., Pons, F., Ba, M., 2016. Flow and performance analysis of H-Darrieus hydroturbine in a confined flow: a computational and experimental study. J. Fluids Struct. 66, 382–402. http://dx.doi.org/10.1016/j.jfluidstructs.2016.08.003.

Gorle, J.M.R., Terjesen, B.F., Mota, V.C., Summerfelt, S.T., 2018. Water velocity in commercial RAS culture tanks for Atlantic salmon smolt production. Aquacult. Eng. 81, 89–100. http://dx.doi.org/10.1016/j.aquaeng.2018.03.001.

Jones, W.P., Launder, B.E., 1972. The prediction of laminarization with a two-equation model of turbulence. Int. J. Heat Mass Transf. 15 (2), 301–314. http://dx.doi.org/10.1016/0017-9310(72)90076-2.

Kawahara, G., Kida, S., Tanaka, M., Yanase, S., 1997. Wrap, tilt and stretch of vortex lines around a strong thin straight vortextube in a simple shear flow. J. Fluid Mech. 353, 115–162. http://dx.doi.org/10.1017/S0022112097007246.

Kim, T., Yoon, H.-S., Shin, S., Oh, M.-H., Kwon, I., Lee, J., Choi, S.-D., Jeong, K.-S., 2015. Physical and biological evaluation of co-culture cage systems for grow-out of juvenile abalone, *Haliotis discus* hannai, with juvenile sea cucumber, *Apostichopus japonicus* (Selenka), with CFD analysis and indoor seawater tanks. Aquaculture 447, 86–101. http://dx.doi.org/10.1016/j.aquaculture.2014.07.001.

Klebert, P., Volent, Z., Rosten, T., 2018. Measurement and simulation of the three-dimensional flow pattern and particle removal efficiencies in a large floating closed sea cage with multiple inlets and drains. Aquacult. Eng. 80, 11–21. http://dx.doi.org/10.1016/j.aquaeng.2017.11.001.

Klimenko, A.Y., 2001. Near-axis asymptote of the bathtub-type inviscid vortical flows. Mech. Res. Commun. 28 (2), 207–212. http://dx.doi.org/10.1016/S0093-6413(01)00164-1.

Lane, G.L., 2017. Improving the accuracy of CFD predictions of turbulence in a tank stirred by a hydrofoil impeller. Chem. Eng. Sci. 169, 188–211. http://dx.doi.org/10.1016/j.ces.2017.03.061.

Launder, B.E., Spalding, D.B., 1974. The numerical computation of turbulent flows. Comput. Methods Appl. Mech. Eng. 3 (2), 269–289. http://dx.doi.org/10.1016/0045-7825(74)90029-2.

Masalo, I., Reig, L., Oca, J., 2008. Study of fish swimming activity using acoustical Doppler velocimetry (ADV) techniques. Aquacult. Eng. 38 (1), 43–51. http://dx.doi.org/10.1016/j.aquaeng.2007.10.007.

Marshall, J.S., Beninati, M.L., 2005. External turbulence interaction with a columnar vortex. J. Fluid Mech. 540 (1), 221–245. http://dx.doi.org/10.1017/S002211200500580X.

Masalo, I., Oca, J., 2014. Hydrodynamics in a multivortex aquaculture tank: effect of baffles and water inlet characteristics. Aquacult. Eng. 58, 69–76. http://dx.doi.org/10.1016/j.aquaeng.2013.11.001.

Meshkov, E.E., Sirotkin, A.A., 2013. Bath-tub vortex attenuation with the increase of in-vessel water level. Phys. Scr. 2013, 014058. http://dx.doi.org/10.1088/0031-8949/2013/T155/014058.

Mizushima, J., Abe, K., Yokoyama, N., 2014. Bathtub vortex induced by instability. Phys. Rev. E 90, 041002. http://dx.doi.org/10.1103/PhysRevE.90.041002.

Nordin, N., Seri, S.M., Taib, I., Mohammed, A.N., Abdullah, M.K., Sapit, A., 2017. Secondary flow vortices and flow separation of 2-D turning diffuser via particle image velocimetry. IOP Conf. Ser.: Mater. Sci. Eng. 226, 012149. http://dx.doi.org/10.1088/1757-899X/226/1/012149.

Oca, J., Masalo, I., 2007. Design criteria for rotating flow cells in rectangular aquaculture tanks. Aquacult. Eng. 36, 36–44. http://dx.doi.org/10.1016/j.aquaeng.2006.06.001.

Oca, J., Masalo, I., 2013. Flow pattern in aquaculture circular tanks: influence of flow rate, water depth, and water inlet & outlet features. Aquacult. Eng. 52, 65–72. http://dx.doi.org/10.1016/j.aquaeng.2012.09.002.

Oca, J., Masalo, I., Reig, L., 2004. Comparative analysis of flow patterns in aquaculture rectangular tanks with different water inlet characteristics. Aquacult. Eng. 31, 221–236. http://dx.doi.org/10.1016/j.aquaeng.2004.04.002.

Paul, T.C., Sayal, S.K., Sakhuja, V.S., Dhillon, G.S., 1991. Vortex-settling basin design considerations. J. Hydraul. Eng. 117, 172–189. http://dx.doi.org/10.1061/(ASCE)0733-9429(1991) 117:2(172).

Pfeiffer, T.J., Riche, M.A., 2011. Evaluation of a low-head Recirculating Aquaculture System used for rearing Florida pompano to market size. J. World Aquacult Soc. 42 (2), 198–208. http://dx.doi.org/10.1111/j.1749-7345.2011.00456.x.

Plew, D.R., Klebert, P., Rosten, T.W., Aspaas, S., Birkevold, J., 2015. Changes to flow and turbulence caused by different concentrations of fish in a circular tank. J. Hydraul. Res. 53 (3), 364–383. http://dx.doi.org/10.1080/00221686.2015.1029016.

Prabhu, P.A.J., Kaushik, S.J., Geuden, I., Stouten, T., Fonta-gné-dicharry, S., Veron, V., Mariojouls, C., Verreth, J.A.J., Eding, E.H., Schrama, J.W., 2017. Water exchange rate in RAS and dietary inclusion of micro-minerals influence growth, body composition and mineral metabolism in common carp. Aquaculture 471, 8–18. http://dx.doi.org/10.1016/j.aquaculture.2016.12.031.

Saba, G.K., Steinberg, D.K., 2012. Abundance, composition, and sinking rates of fish fecal pellets in the Santa Barbara Channel. Sci. Rep. 2, 716. http://dx.doi.org/10.1038/srep00716.

Schmitt, F.G., 2007. About Boussinesq's turbulent viscosity hypothesis: historical remarks and a direct evaluation of its validity. Comptes Rendus Mécanique 335 (9–10), 617–627. http://dx.doi.org/10.1016/j.crme.2007.08.004.

Shih, T.-S., Liou, W.W., Shabbir, A., Yang, Z., Zhu, J., 1995. A new k-ϵ eddy viscosity model for high Reynolds number turbulent flows. Comput. Fluids 24 (3), 227–238. http://dx.doi.org/10.1016/0045-7930(94)00032-T.

Summerfelt, S.T., Davidson, J.W., Waldrop, T.B., Tsukuda, S.M., Williams, J.B., 2004. A

partial-reuse system for coldwater aquaculture. Aquacult. Eng. 31 (3–4), 157–181. http://dx.doi.org/10.1016/j.aquaeng.2004.03.005.

Summerfelt, S.T., Davidson, J., Wilson, G., Waldrop, T., 2009b. Advances in fish harvest technologies for circular tanks. Aquacult. Eng. 40 (2), 62–71. http://dx.doi.org/10.1016/j.aquaeng.2008.12.001.

Summerfelt, S.T., Mathisen, F., Holan, A.B., Terjesen, B.F., 2016. Survey of large circular and octagonal tanks operated at Norwegian commercial smolt and post-smolt sites. Aquacult. Eng. 74, 105–110. http://dx.doi.org/10.1016/j.aquaeng.2016.07.004.

Summerfelt, S.T., Sharrer, M., Gearheart, M., Gillette, K., Vinci, B.J., 2009a. Evaluation of partial water reuse systems used for Atlantic salmon smolt production at the White River National Fish Hatchery. Aquacult. Eng. 41, 78–84. http://dx.doi.org/10.1016/j.aquaeng.2009.06.003.

Summerfelt, S.T., Sharrer, M., Marshall, C., Obaldo, O., 2006. Controlling water velocity across large 'Cornell-type' dual-drain culture tanks. In: 6th International Recirculating Aquaculture Conference, July 20–23, Roanoke, Virginia, pp. 382–393.

Terjesen, B.F., Summerfelt, S.T., Nerland, S., Ulgenes, Y., Fjæra, S.O., Reiten, B.K.M., Selset, R., Kolarevic, J., Brunsvik, P., Bæverfjord, G., Takle, H., Kittelsen, A.H., Åsgård, T., 2013. Design, dimensioning, and performance of a research facility for studies on the requirements of fish in RAS environments. Aquacult. Eng. 54, 49–63. http://dx.doi.org/10.1016/j.aquaeng.2012.11.002.

Tvinnereim, K., Skybakmoen, S., 1989. Water exchange and self-cleaning in fish rearing tanks. In: De Pauw, N., Jaspers, E., Ackefors, H., Wilkens, N. (Eds.), Aquaculture: A Biotechnology in Progress. European Aquaculture Society, Bredena, Belgium, pp. 1041–1047.

Veerapen, J.P., Lowry, B., Couturier, M.F., 2005. Design methodology for the swirl separator. Aquacult. Eng. 33, 21–45. http://dx.doi.org/10.1016/j.aquaeng.2004.11.001.

Venegas, P.A., Narvaez, A.L., Arriagada, A.E., Llancaleo, K.A., 2014. Hydrodynamic effects of use of eductors (Jet-Mixing Eductor) for water inlet on circular tank fish culture. Aquacult. Eng. 59, 13–22. http://dx.doi.org/10.1016/j.aquaeng.2013.12.001.

Wolters, W., Masters, A., Vinci, B., Summerfelt, S., 2009. Design, loading, and water quality in recirculating systems for Atlantic Salmon (*Salmo salar*) at the USDA ARS National Cold Water Marine Aquaculture Center (Franklin, Maine). Aquacult. Eng. 41 (2), 60–70. http://dx.doi.org/10.1016/j.aquaeng.2009.06.011.